2020년 2월

박사학위 논문

Fabrication and Characterization of Porous Silicon Nanowires

조 선 대 학 교 대 학 원

화 학 과

정 대 윤

Fabrication and Characterization of Porous Silicon Nanowires

다공성 실리콘 나노와이어의 제작과 특성분석

2020년 2월 25일

조 선 대 학 교 대 학 원

화 학 과

정 대 윤

Fabrication and Characterization of Porous Silicon Nanowires

지도교수 손 홍 래

이 논문을 이학박사학위신청 논문으로 제출함.

2019년 10월

조 선 대 학 교 대 학 원

화 학 과

정 대 윤

정대윤의 박사학위논문을 인준함

위원장 조선대학교 교수 이 범 규 (인)

위 원 조선대학교 교수 고 문 주 (인)

위 원 조선대학교 교수 손 홍 래 (인)

위 원 조선대학교 교수 김 호 중 (인)

위 원 세한대학교 교수 고 영 춘 (인)

2019년 12월

조 선 대 학 교 대 학 원

TABLE OF CONTENTS

TABLE OF CONTENTS i
LIST OF SYMBOLS AND ABBREVIATIONS ii
LIST OF FIGURES iii
ABSTRACT v

PART 1

Fabrication and Characterization of Porous Silicon Nanowires

1.1. Introduction 2

1.2. Experiments..... 4

1.3. Results and Discussion 6

1.4.. Conclusion 12

1.5. Reference 13

PART 2

Origin of Luminescence from Oxidized Silicon Nanowires

2.1. Introduction 18

2.2. Experiments..... 20

2.3. Results and Discussion 22

2.4. Conclusion 27

2.5. Reference 28

LIST OF SYMBOLS AND ABBREVIATIONS

SiNWs	Silicon Nanowires
MACE	Metal-Assisted Chemical Etching
ECE	Electro Chemical Etching
HR-TEM	High-resolution Transmission Electron Microscopy
HF	Hydrofluoric Acid
H_2O_2	Hydrogen peroxide
$AgNO_3$	Silver nitrate
Si	Silicon
μm	Micrometer
mA	Milliampere
cm	Centimeter
cm^2	Square Centimeter
min	Minute
Ag	Silver
HNO_3	Nitric Acid
SiO_2	Silicon Dioxide
nm	Nanometer
FE-SEM	Field Emission-Scanning Electron Microscope
M	Molarity
Ω	Ohm
Å	Angstrom
PSi	Porous Silicon
CCD	Charge-Coupled Device
PL	Photoluminescence
UV	Ultraviolet
HeCd	Helium-Cadmium
h	Hour
K	Kelvin
cm^{-1}	Typically Centimeters

LIST OF FIGURES

PART 1

Fabrication and Characterization of Porous Silicon Nanowires

Figure 1.1. Schematic diagram of the synthesis of porous SiNWs

Figure 1.2. Cross-sectional SEM images of (a-c) the porous silicon with the etching times of (a) 5 min; (b) 10 min; (c) 30 min, and (d-f) the SiNWs with the etching times of (d) 20 min; (e) 30 min; (f) 40 min

Figure 1.3. Plot of etching depth vs. etching time of the porous silicon, SiNW, and porous SiNW

Figure 1.4. Surface and cross-section SEM images of (a-b) the porous silicon and (c-d) the porous SiNW prepared from the as-prepared porous silicon

Figure 1.5. Cross-section SEM images of (a) the porous SiNWs produced by using the porous silicon etched for 10 min, and (b) its enlarged image

Figure 1.6. HR-TEM images of the SiNW (a and b) and the porous SiNW (c and d). the selected area electron diffraction patterns (insets) confirm the single crystalline nature along their length

PART 2

Origin of Luminescence from Oxidized Silicon Nanowires

Figure 2.1. Evolution of the PL from the Si NWs. The insets show photographs of the Si NWs under white light (left)

Figure 2.2. Surface and cross-sectional SEM images of the Si NWs

Figure 2.3. **High-resolution SEM images of (a) a non-luminescent Si NW and (b) a luminescent Si NW**

Figure 2.4. **HR-TEM images of a luminescent Si NW. The inset shows the selected area electron diffraction patterns**

Figure 2.5. **Temperature dependence of the PL spectra from Si NWs**

Figure 2.6. **Raman spectra of non-luminescent and luminescent Si NWs. The inset shows that the first-order Raman peak of the luminescent Si NWs is downshifted by 5.8 cm^{-1}**

초 록

다공성 실리콘 나노와이어의 제작과 특성분석

박사과정 : 정 대 윤
지도교수 : 손 홍 래
조선대학교 화학과

실리콘 나노와이어는 나노스케일의 전자소재, 열전변환, 광전지, 배터리 전극, 전자 바이오센서, 전계효과 트랜지스터 등 여러 분야로의 활용으로 각광받고 있는 연구 분야이다. 실리콘 기반의 물질들은 풍부한 매장량과 독성이 없으며 생산 제작과정에 있어 비용이 저렴하며 수득률이 높아 관심이 높다.
최근 여러 실리콘 나노와이어의 제작 기술이 발전되어 왔다. 대표적인 예로는 기상-액상-고상 성장 (Vapor-Liquid-Solid growth, VLS), 화학적 또는 물리적 증착법, 전자빔 증착법으로 제작 될 수 있다. 하지만 이러한 방법들은 높은 온도, 복잡한 장비와 격렬한 조건과 성장 속도가 느리며 가격이 높다는 단점이 있다.

최근 금속을 이용한 화학적 식각(Metal-Assisted Chemical Etching, MACE)가 단순하고 낮은 제작온도, 저렴한 제작비용과 대면적 제작이 가능해 실리콘 나노와이어를 제작하는데 널리 사용되고 있다. 실리콘 웨이퍼 위에 금속 나노입자들을 전기도금을 통해 형성시키고 이 입자들이 산화/환원 반응을 촉진시키는 촉매로 사용되는데 표면에 도금된 은 입자들과 실리콘 웨이퍼 접촉면에

서 촉매현상으로 실리콘이 산화되어 HF에 의해 식각되고 결과적으로 남게 되는 기벽이 나노와이어 형태를 만들게 된다. 이 때 실리콘 나노와이어의 형태를 결정짓는 요소들은 도핑 유형, 도핑 레벨, 실리콘 웨이퍼의 결정 방향과 과산화수소의 농도와 식각 온도 등 다양하다.

다공성 실리콘 나노와이어는 비표면적이 매우 높아 화학적, 생물학적 센서, 약물전달체, 의학적 진단과 같이 넓은 분야로의 활용이 가능해 특히 관심 받고 있는 연구 분야이다.

배터리 음극제로써의 실리콘 나노와이어 전극은 높은 충전 용량과 용량 유지율을 기대할 수 있다. 특히 다공성 실리콘 나노와이어는 충전 용량과 용량 유지율을 높이고 특히 리튬 이온의 삽입과 추출 과정에서 리튬-실리콘의 부피 팽창 문제를 크게 완화시킬 수 있다. 하지만 지금까지의 다공성 실리콘 나노와이어를 제작하는 방법은 식각용액의 과산화수소의 농도를 조절하면서 다공성도를 조절하는 것이었다. 이에 본 연구에서는 다공성 실리콘을 이용하여 금속을 이용한 화학적 식각을 통한 실리콘 나노와이어의 표면과 내부에도 기공을 가지는 다공성 실리콘 나노와이어를 효율적으로 제작하는 방법에 대하여 연구하였다.

또한 최근 Voigt가 MACE를 통한 실리콘 나노와이어의 가시광선 영역에서 나오는 발광현상에 관하여 보고하였지만 발광현상이 실리콘 나노와이어에서 나오는 것인지는 명확하게 증명하지는 못하였다. 이에 본 연구에서 MACE를 통해 만들어진 발광현상을 가진 실리콘 나노와이어를 제작하여 실리콘 나노와이어에서 나오는 발광현상의 기원을 증명하고자 5 K에서 300 K까지 다양한 온도에서 광학적 특성을 분석하였다.

Part 1

Fabrication and Characterization of Porous Silicon Nanowires

1.1. Introduction

Considerable interest has been shown in the research and development of silicon nanowires (SiNWs) for various applications in the fields of nanoscale electronics,[1-3] thermoelectric,[4] photovoltaics,[5-8] battery electrodes,[9] electronic biosensors,[10] and field-effect transistors.[11-13] Silicon-based materials are strongly favored due to their material abundance and nontoxicity leading to low production/processing cost and high production yield.[14,15] In recent years, many synthesis techniques for SiNWs have been developed. The synthesis of SiNWs can be achieved using metal-catalyzed growth, known as vapor-liquid-solid growth,[16] chemical vapor deposition or physical vapor deposition method,[17] or electron beam evaporation.[18-21] These methods are quite accessible and well controlled. However, these techniques often require hazardous silicon precursors, high temperature, complex equipment, and other vigorous conditions. In addition, the growth of SiNWs is very slow and the cost is high.

Recently, metal-assisted chemical etching (MACE) has been widely used for the synthesis of SiNWs, because this technique has advantages such as simplicity, low operating temperature, and low cost.[22,23] Pt, Au, Pd, Cu, and Ni depositions on silicon wafers in HF solution have been extensively studied.[24-26] MACE is a localized microelectrochemical redox reaction process in which both anodic and cathodic processes occur simultaneously on the silicon surface, involving the spontaneous oxidation of silicon atoms and the reduction of metal ions to metallic particles in the absence of an external source of electric current. The morphologies of SiNWs can be affected by many factors such as doping type, doping level, orientation of silicon wafers, concentration of H_2O_2 in the etchant, and etching temperature.

Porous silicon has been intensively investigated for a variety of applications such as chemical and biological sensors, drug delivery carriers, and medical diagnostics, since it has a very large specific surface area in the order of a few hundreds of m^2/cm^3, corresponding to about one thousand times the surface area of a polished silicon wafer.[27-37] The direction and size of

pores depend on surface orientation, doping level, doping type, temperature, current density, and the composition of etching solution.

For an application of battery electrodes, the SiNW anode showed larger charge capacity and longer cycling stability than conventional planar-polished Si wafers.[38,39] Porous SiNWs would be ideal to further enhance charge capacity and cycling stability, by alleviating volume change of Li-Si alloy during lithium insertion and extraction. However, to our knowledge, only one method for the synthesis of porous SiNWs has been presented in literatures, where hydrogen peroxide concentration in the etching solution is varied to control porosity.[40,41] Here, we report an efficient synthetic route producing porous SiNWs through the MACE of porous silicon.

1.2. Experiments

1.2.1. Materials

HF (48 - 51%, ACS Reagent, J.T. Baker, PA, USA), H_2O_2 (30%, ACS Reagent, Sigma-Aldrich, St. Louis, MO, USA), HNO_3 (70%, ACS Reagent, Sigma-Aldrich), acetone (99.9%, ACS Reagent, Sigma-Aldrich), ethanol (99.8%, Merck, Darmstadt, Germany), and $AgNO_3$ (>99.995%, Alfa Aesar, Massachusetts, USA), silicon (100) wafer (Prime grade, Siltronix Inc., Archamps, France) were used as received.

1.2.2. Preparation of porous silicon

Si (100) wafers (p-type, boron-doped, 1 - 10 Ω·cm, 500 μm thick) were used to fabricate porous silicon by anodic electrochemical etching (ECE) in ethanolic HF consisted of a 1:1 volume mixture of aqueous 48% hydrofluoric acid and absolute ethanol. The galvanostatic etch was carried out in a Teflon cell using a two-electrode configuration with a Pt counter electrode. Porous silicon samples were prepared at an anodization current of 30 mA/cm^2 for 3, 5, 10, 20, and 30 min, respectively. The anodization current was supplied by a Keithley 2420 high-precision constant current source (Keithley Instruments Inc., Cleveland, OH, USA). All samples were then rinsed several times with ethanol and dried under argon atmosphere prior to use.

1.2.3. Preparation of porous SiNWs

After the electrochemical etching, Ag nanoparticles were spin-coated on the as-prepared porous silicon, by using the Ag-coating solution containing 4.8 M HF and 0.04 M $AgNO_3$. After the Ag-nanoparticle coating, the porous silicon was washed with water to remove extra Ag^+ ions and then immersed in the oxidizing HF etching solution composed of 4.8 M HF and 30% H_2O_2 (10:1 v/v) in a reaction vessel. After the etching at room temperature, the porous SiNWs were washed repeatedly with water and then immersed in dilute HNO_3 (1:1 v/v) to

dissolve the Ag catalyst. The porous SiNW samples were rinsed with deionized water and dried at room temperature; their surfaces were colored deep black and their rear sides were colored gray. To obtain transmission electron microscopy (TEM) images, the porous SiNWs were sonicated in ethanol. The TEM specimens were prepared by dipping carbon micro-grids (Ted Pella Inc., 200 Mesh Copper Grid) into the ethanol solution.

1.2.4. Preparation of SiNWs

The silicon wafers were cut into 10 mm^2 pieces and cleaned by rinsing in acetone for 2 min followed by an ethanol rinse for another 2 min. Native SiO_2 removal was carried out by brief dipping in 48% HF solution followed by 2% HF rinsing for 1 min. Finally, the samples were rinsed in deionized water and blow-dried with nitrogen. This cleaning procedure yields hydrogen-terminated silicon surfaces (for a limited time of a few minutes), which allowed for subsequent silver deposition on oxide free silicon wafer surfaces. Then the method described for the porous SiNWs using the silicon wafers instead of porous silicon was followed.

1.2.5. Instrumentation and data acquisition

Morphologies of porous silicon and porous SiNWs were obtained by a cold field emission scanning electron microscopy (FE-SEM, S-4800, Hitachi). The high resolution TEM employed in this work is a Philips TECNAI F20 microscope operating at 200 keV.

1.3. Results and Discussion

Porous silicon has been intensively investigated for a variety of applications based on porosity, since it has a very large specific surface area in the order of a few hundreds of m^2/cm^3, corresponding to about one thousand times the surface area of a polished silicon wafer. The electrochemical process generates a uniform layer of porous silicon; the thickness and porosity of a given layer is controlled by the current density, the etching duration, and the composition of the etchant solution. The SiNWs as lithium-ion battery anodes showed a larger charge capacity,[36] However, they still exhibited a volume expansion problem during the lithium insertion and extraction process. Porous SiNWs, the combination of porous silicon and SiNW, would be an ideal candidate for lithium-ion battery anodes and were fabricated through the MACE of porous silicon with silver nanoparticles. In our experiment, an anodic etch of p-type silicon wafer with resistivities of 1 - 10 Ω·cm in ethanolic HF solution generally produces a porous silicon single layer with a network of micropores, rather than mesopores or macropores. The average pore size of the p-type porous silicon was about 3 nm. The as-prepared porous silicon was used to fabricate porous SiNWs through MACE.

Figure 1 shows the schematic diagram for the synthesis of porous SiNWs through the MACE of porous silicon with silver nanoparticles.

Figure 2 shows the SEM cross-section images of the porous silicon and the SiNWs, with different etching times. The growth of porous silicon as shown in Figs. 2(a), 2(b), and 2(c) was obtained with the etching times of 5, 10, and 30 min, respectively. The growth of SiNWs as shown in Figs. 2(d), 2(e), and 2(f) was obtained with the etching times of 20, 30, and 40 min, respectively. Finally, the growth of porous SiNWs was obtained using the as-grown porous silicon (20 min) with etching times of 20, 30, and 40 min, respectively.

Figure 3 shows the plot of etching depth vs. etching time to obtain the etching rates of the porous silicon, SiNW, and porous SiNWs, respectively. The etch rates were observed to be ~1.0 μm/min and ~0.42 μm/min for the porous silicon and the SiNWs, respectively. The etch rate of the porous SiNWs was slightly faster than that of SiNWs and was about 0.48 μm/min.

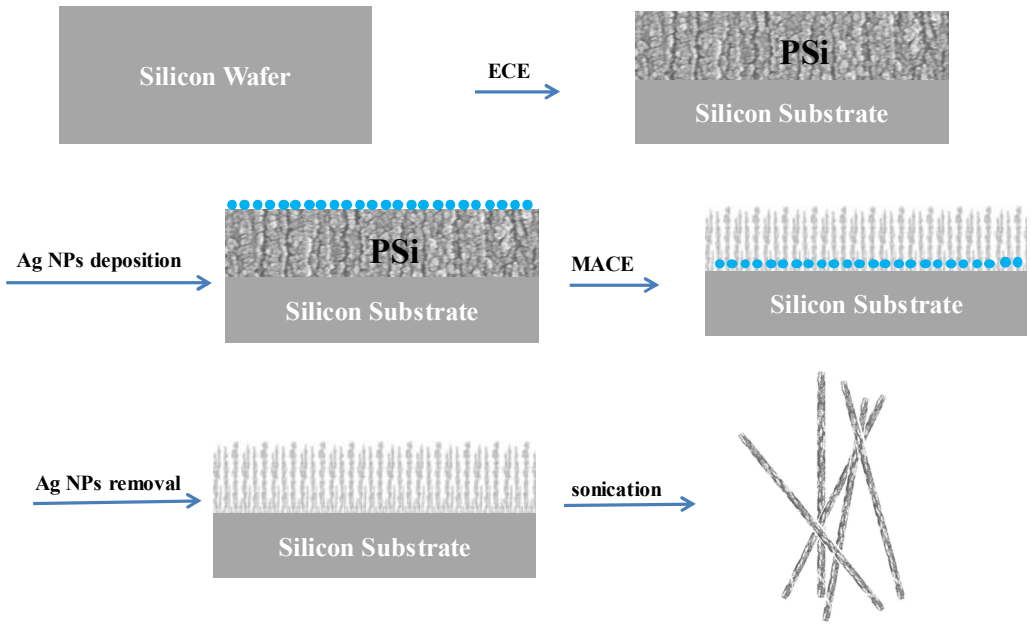

Fig. 1.1. Schematic diagram of the synthesis of porous SiNWs.

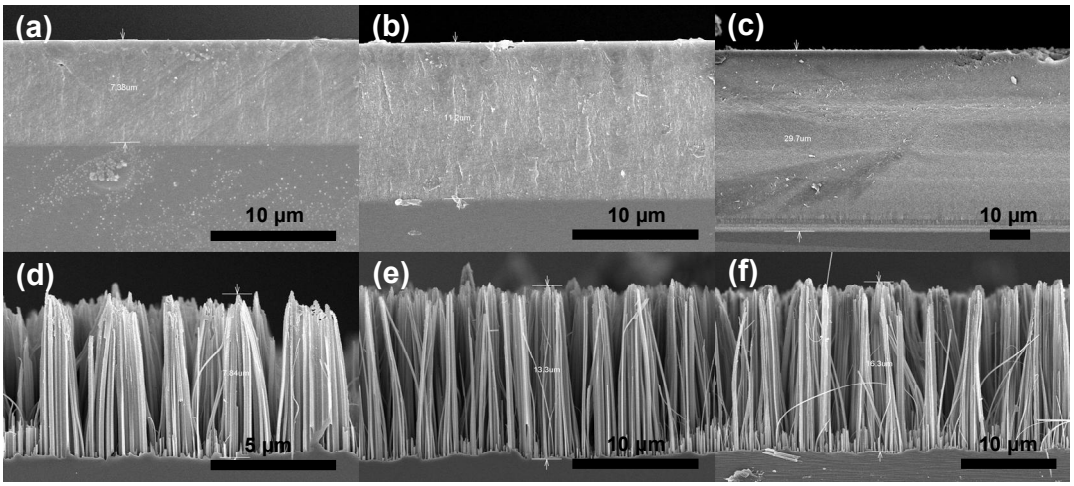

Fig. 1.2. Cross-sectional SEM images of (a-c) the porous silicon with the etching times of (a) 5 min; (b) 10 min; (c) 30 min, and (d-f) the SiNWs with the etching times of (d) 20 min; (e) 30 min; (f) 40 min.

Peng et al. reported that the formation of vertically aligned NWs in metal-assisted etch is due to the confined etch near the silver nanoparticles, in which the silver nanoparticles on the silicon surface catalyze the etching reaction and thus create nanopits.[42] Qu et al. reported that the highly doped wafers, which have many defective sites, have too high density of nucleated silver nanoparticles on the surface that are in close proximity to each other, and each nanoparticle may not be effectively confined in its own pits to ensure vertical etching.[40]

However, the porous silicon has pores as defective sites on the silicon surface, and the initial nucleation of silver nanoparticles may occur near pore sites where the energy barrier for redox reaction is lower and each silver nanoparticle may be effectively confined in its own pores to ensure vertical etching. Then, the pore structure in the porous layer might increase the etching speed of SiNWs compared to crystalline silicon wafers.

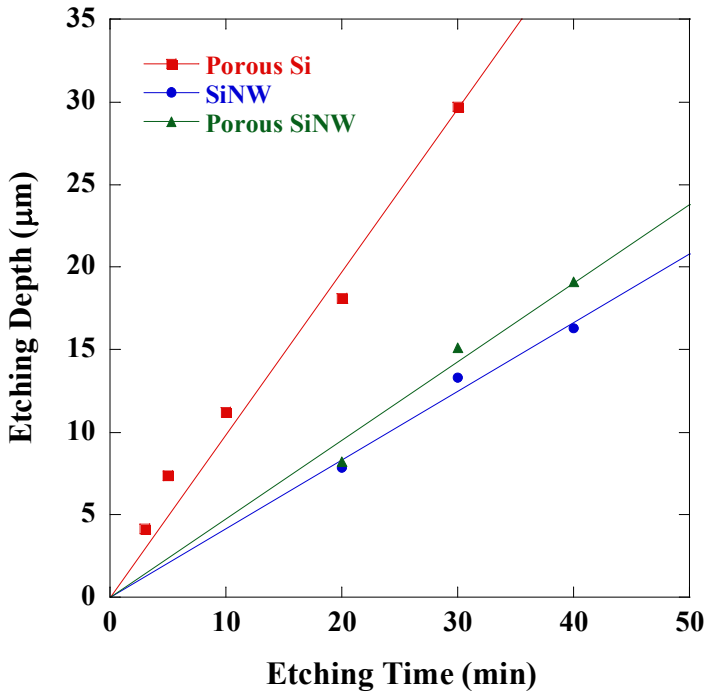

Fig. 1.3. Plot of etching depth vs. etching time of the porous silicon, SiNW, and porous SiNW.

The surface and cross-section SEM images of the porous silicon etched for 3 min are shown in Figs. 4(a) and 4(b). The pore size of the porous silicon is less than 4 nm and the depth is about 4.0 μm. Surface and cross-section SEM images of the porous SiNWs are shown in Figs. 4(c) and 4(d), which indicate that the porous SiNWs distribute uniformly on the entire porous silicon layer and are vertical to the substrate surface. The tips of the porous SiNWs congregate together, and the diameters of the congregated bundles are 2 to 4 μm. The length of the porous SiNWs is about 4.5 μm which is very close to the depth of the as prepared porous silicon shown in Fig. 4(b).

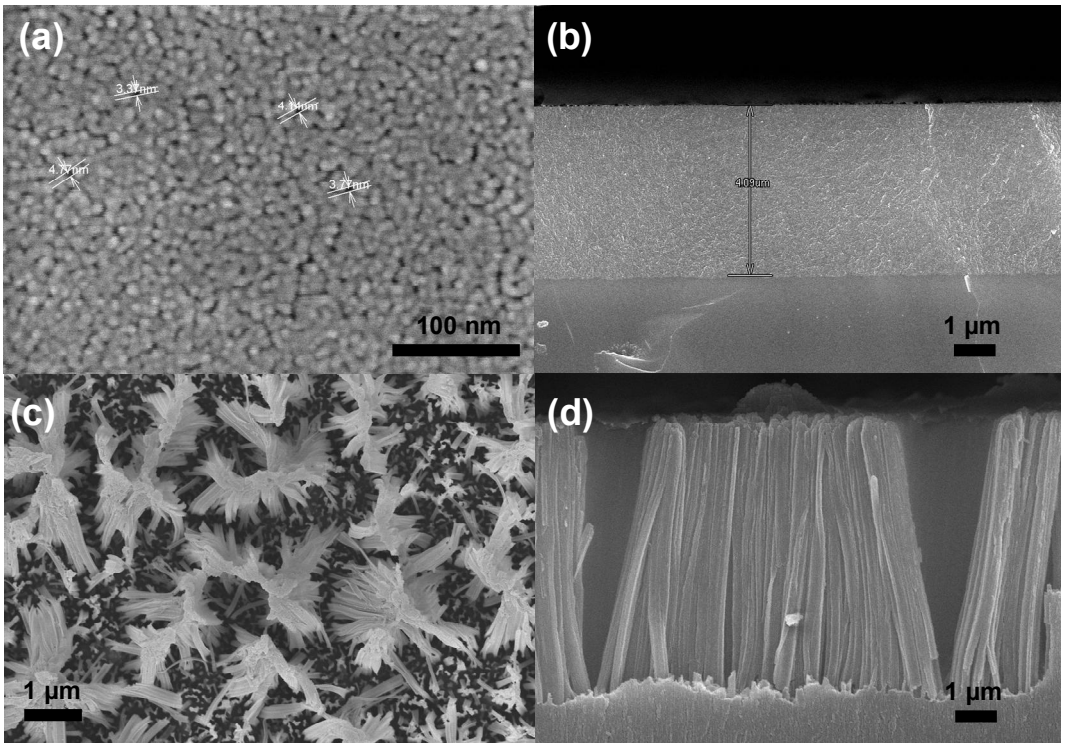

Fig. 1.4. Surface and cross-section SEM images of (a-b) the porous silicon and (c-d) the porous SiNW prepared from the as-prepared porous silicon.

Figures 5(a) and 5(b) show the cross-section SEM image of the porous SiNWs etched for 30 min with the porous silicon prepared at the anodization current of 30 mA/cm^2 for 10 min and its enlarged image, respectively. The depth of the electrochemically etched porous silicon for 10 min is about 11.2 ㎛ and the length of the electroless etched porous SiNWs from the as-prepared porous silicon for 30 min is about 11.7 ㎛. These studies clearly demonstrate that the enlarged SEM image of the porous SiNW displays entirely porous structures. Qu et al. reported that the SiNWs first become rough on the surface, then start to evolve porous shells surrounding the solid cores, and eventually form entirely porous NWs with an increase of H_2O_2 concentration.[40] However, no direct evidence has been found for the entire formation of porous SiNWs. In our studies, the porous silicon is employed for the generation of SiNWs of which the structures are already porous.

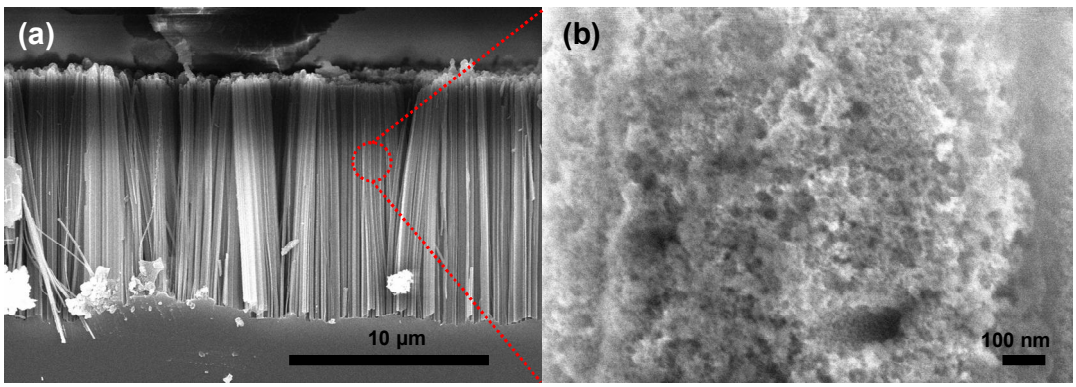

Fig. 1.5. Cross-section SEM images of (a) the porous SiNWs produced by using the porous silicon etched for 10 min, and (b) its enlarged image.

Figure 6 shows the HR-TEM images of the as-grown SiNW and porous SiNW. The as-grown SiNWs shown in Fig. 6(a) have a thin rough surface on the solid core, but the porous silicon NW shown in Fig. 6(c) exhibits an entirely porous structure with the rough surface. The selected area electron diffraction (SAED, inset) patterns indicate that the SiNW and porous SiNW are single crystalline along their length. The lattice plane image shows typical Si (100),

and the measured *d* spacing is 2.86 Å for (100). The localized lattice fringe and the single crystal-like diffraction pattern shown in Fig. 6(b) are observed in the SiNWs. Figures 6(c) and 6(d) demonstrate that the porous SiNWs retain the single crystalline structure of the starting silicon wafer with a sponge-like porous structure. The diameters of the lateral pores of the porous SiNWs shown in Fig. 6(c) are less than 5 nm.

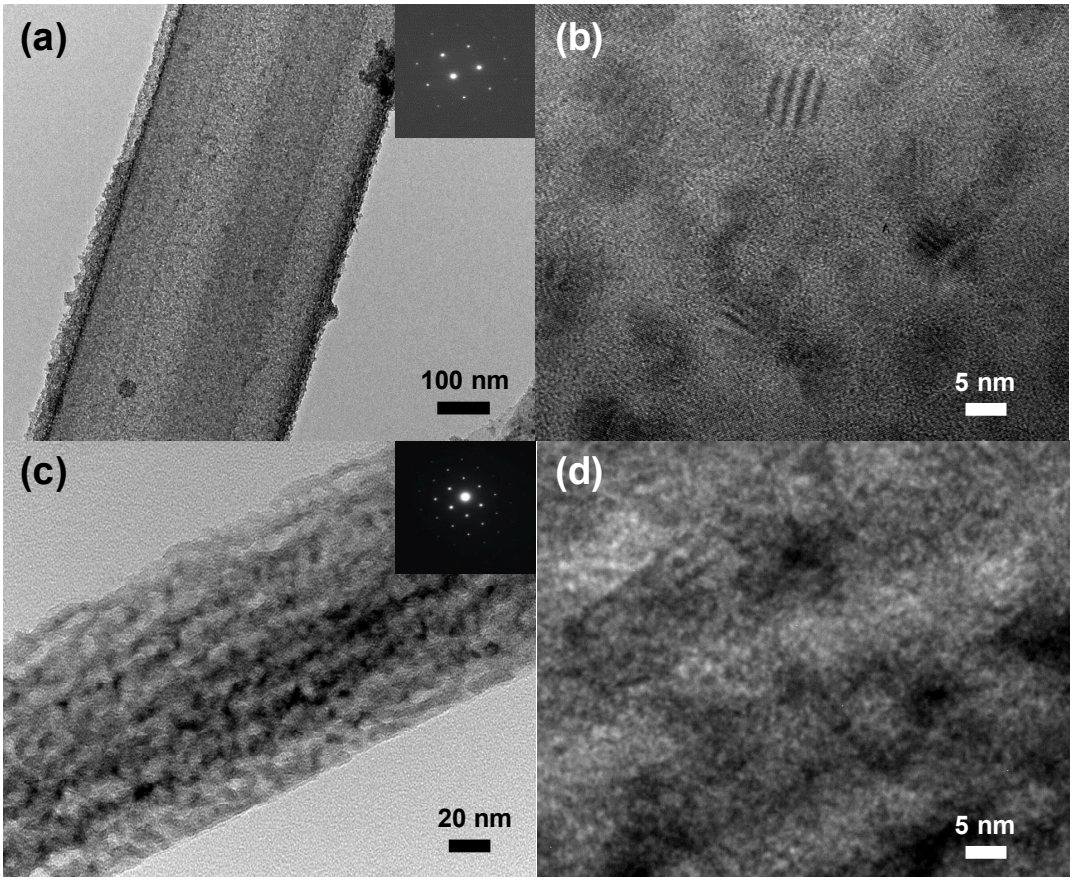

Fig. 1.6. HR-TEM images of the SiNW (a and b) and the porous SiNW (c and d). the selected area electron diffraction patterns (insets) confirm the single crystalline nature along their length.

1.4. Conclusion

We demonstrated that porous SiNWs were successfully synthesized through MACE of porous silicon with silver nanoparticles. The etching rates of the porous silicon, SiNW, and porous SiNW were obtained with different etching times. The etch rate of the porous SiNWs was slightly faster than that of the SiNWs but slower than that of porous silicon. The surface and cross-section SEM images of the porous SiNWs indicated that the porous SiNWs distributed uniformly on the entire porous silicon layer and the tips of the porous SiNWs congregated together. The HR-TEM images indicated that the as-grown SiNWs had a thin rough surface on the solid core, but the porous SiNW exhibited an entirely porous structure with the rough surface. The porous SiNW retained the single crystalline structure of the starting silicon wafer with the sponge-like porous structure, and the diameters of lateral pores were less than 5 nm.

1.5. References

[1] Y. Huang, X. Duan, Y. Cui, L. J. Lauhon, K.-H. Kim, and C. M. Lieber, *Science* **294**, 1313 (2001).

[2] T. Moon, J. Kang, Y. Han, C. Kim, Y. Jeon, H. Kim, and S. Kim, *ACS Appl. Mater. Interfaces* **3**, 3957 (2011).

[3] T. Moon, J.-C. Jung, Y. Han, Y. Jeon, S.-M. Koo, and S. Kim, *IEEE T. Electron Dev.* **59**, 3288 (2012).

[4] A. I. Hochbaum, R. Chen, R. D. Delgado, W. Liang, E. C. Garnett, M. Najarian, A. Majumdar, and P. Yang, *Nature* **451**, 163 (2008).

[5] B. Tian, X. Zheng, T. J. Kempa, Y. Fang, N. Yu, G. Yu, J. Huang, and C. M. Lieber, *Nature* **449**, 885 (2007).

[6] E. C. Garnett and P. Yang, *J. Am. Chem. Soc.* **130**, 9224 (2008).

[7] M. D. Kelzenberg, D. B. Turner-Evans, B. M. Kayes, M. A. Filler, M. C. Putnam, N. S. Lewis, and H. A. Atwater, *Nano Lett.* **8**, 710 (2008).

[8] K. Bhowmik and A. Mondal, *Electron. Mater. Lett.* **11**, 180 (2015).

[9] C. K. Chan, H. Peng, G. Liu, K. McIlwrath, X. F. Zhang, R. A. Huggins, and Y. Cui, *Nat. Nanotechnol.* **3**, 31 (2008).

[10] G. Zheng, F. Patolsky, Y. Cui, W. U. Wang, and C. M. Lieber, *Nat. Biotechnol.* **23**, 1294 (2005).

[11] S. M. Koo, Q. Li, M. D. Edelstein, C. A. Richter, and E. M. Vogel, *Nano Lett.* **5**, 2519 (2005).

[12] Y. Cui, Z. Zhong, D. Wang, W. U. Wang, and C. M. Lieber, *Nano Lett.* **3**, 149 (2003).

[13] X. F. Duan, Y. Huang, and C. M. Lieber, *Nano Lett.* **2**, 487 (2002).

[14] T. Moon, G. S. Shin, and B. Park, *Electron. Mater. Lett.* **11**, 917 (2015).

[15] W. Lee, T. Hwang, S. Lee, S.-Y. Lee, J. Kang, B. Lee, J. Kim, T. Moon, and B. Park, *Nano Energy* **17**, 180 (2015).

[16] R. S. Wagner and W. C. Ellis, *Appl. Phys. Lett.* **4**, 89 (1964).

[17] Y. Wang, V. Schmidt, S. Senz, and U. Gosele, *Nat. Nanotechnol.* **1**, 186 (2006).

[18] V. Sivakov, F. Heyroth, F. Falk, G. Andra, and S. Christiansen, *J. Cryst. Growth* **300**, 288 (2007).

[19] V. Sivakov, G. Andra, C. Himcinschi, U. Gosele, D. R. T. Zahn, and S. Christiansen, *Appl. Phys. A Mater. Sci. Process.* **85**, 311 (2006).

[20] B. Fuhrmann, H. S. Leipner, H.-R. Hoche, L. Schubert, P. Werner, and U. Gosele, *Nano Lett.* **5**, 2524 (2005).

[21] S. H. Oh, K. van Benthem, S. I. Molina, A. Y. Borisevich, W. Luo, P. Werner, N. D. Zakharov, D. Kumar, S. T. Pantelides, and S. J. Pennycook, *Nano Lett.* **8**, 1016 (2008).

[22] T. Moon, L. Chen, S. Choi, C. Kim, and W. Lu, *Adv. Func. Mater.* **24**, 1949 (2014).

[23] T. Kawashima, T. Mizutani, T. Nakagawa, H. Torii, T. Saitoh, K. Komori, and M. Fujii, *Nano Lett.* **8**, 362 (2008).

[24] K. Q. Peng, Y. J. Yan, S. P. Gao, and J. Zhu, *Adv. Mater.* **14**, 1164 (2002).

[25] K. Peng, J. Hu, Y. Yan, Y. Wu, H. Fang, Y. Xu, S. Lee, and J. Zhu, *Adv. Funct. Mater.* **16**, 387 (2006).

[26] K. Peng, Y. Xu, Y. Wu, Y. Yan, S. T. Lee, and J. Zhu, *Small* **1**, 1062 (2005).

[27] H. Sohn, S. Letant, M. J. Sailor, and W. C. Trogler, *J. Am. Chem. Soc.* **122**, 5399 (2000).

[28] S. Jang, J. Kim, Y. Koh, Y. C. Ko, H.-G. Woo, and H. Sohn, *J. Nanosci.*

Nanotechnol. **7**, 4049 (2007).

[29] S. Jang, Y. Koh, J. Kim, J. Park, C. Park, S. J. Kim, S. Cho, Y. C. Ko, and H. Sohn, *Mater. Lett.* **62**, 552 (2008).

[30] S. G. Kim, S. Kim, Y. C. Ko, S. Cho, and H. Sohn, *Colloids Surfaces A Physicochem. Eng. Asp.* **313**, 398-401, (2008).

[31] Y. Koh, J. Park, J. Kim, S. Jang, H.-G. Woo, and H. Sohn, *J. Nanosci. Nanotechnol.* **10**, 3590 (2010).

[32] S. G. Lee, Y. Koh, S. Jang, J. Kim, H.-G. Woo, S. Kim, and H. Sohn, *J. Nanosci. Nanotechnol.* **10**, 3266 (2010).

[33] V. S. Lin, K. Motesharei, K. P. Dancil, M. J. Sailor, and M. R. Ghadiri, *Science* **278**, 840 (1997).

[34] Y. Koh, S. Jang, J. Kim, S. Kim, Y. C. Ko, S. Cho, and H. Sohn, *Colloids Surfaces A Physicochem. Eng. Asp.* **313** 328-331, (2008).

[35] C. Park, J. Kim, S. Jang, H.-G. Woo, Y. C. Ko, and H. Sohn, *J. Nanosci. Nanotechnol.* **10**, 3375 (2010).

[36] E. Angelin, L. Cheng, W. Freeman, and M. Sailor, *Adv. Drug Deliv. Rev.* **60**, 1266 (2008).

[37] S. Kim, M. S. Kim, H. Park, G. Nam, H. Yoon, and J.-Y. Leem, *Electron. Mater. Lett.* **10**, 565 (2014).

[38] K. Peng, J. Jie, W. Zhang, and S.-T. Lee, *Appl. Phys. Lett.* **93**, 033105 (2008).

[39] T. Moon, C. Kim, and B. Park, *J. Power Sources* **155**, 391 (2006).

[40] Y. Qu, L. Liao, Y. Li, H. Zhang, Y. Huang, and X. Duan, *Nano Lett.* **9**, 4539 (2009).

[41] A. I. Hochbaum, D. Gargas, Y. J. Hwang, and P. Yang, *Nano Lett.* **9**, 3550 (2009).

[42] K. Peng, H. Fang, J. Hu, Y. Wu, J. Zhu, Y. Yan, and S. Lee, *Chem. Eur. J.* **12**, 7942 (2006).

Part 2

Origin of Luminescence from Oxidized Silicon Nanowires

2.1. Introduction

Silicon is the most important semiconducting material for modern industrial applications. Because bulk crystalline silicon has an indirect band gap, it has serious limitations for light-emitting and photonics applications due to its poor emitting property. Considerable interest has been shown in the research and development of nanoscale silicon materials in order to overcome this limitation. Nanoscale silicon materials are found to be good emitters at visible wavelengths due to the quantum confinement of Si [1-3]. The nanoscale Si materials with sizes under 7 ‐ 8 nm, including porous silicon (PSi) [4,5], Si NWs [6-8], and silicon nanocrystals (Si NCs) [9,10], exhibit an excitonic emission due to quantum confinement. Especially, Si NWs have revealed particular attention because of their various applications in the fields of nanoscale electronics [2], thermoelectronics [11], photovoltaics [12-15], battery electrodes [16], electronic biosensors [17], and field-effect transistors [18-20].

In recent years, many synthesis techniques for Si NWs, such as chemical-vapor deposition (CVD) [21], and solid-liquid-solid (SLS) [22,23], vapor-solid-solid (VSS) [24], and electron beam evaporation processes [25], have been developed to grow Si NWs. However, most of those methods require expensive, high-temperature, complex equipment, the use of potentially dangerous silicon precursors, and other vigorous conditions. With these techniques, the Si NWs are mostly crystalline Si and can exhibit luminescence at visible wavelengths when their diameters are below 10 nm. Recently, The metal-assisted chemical-etching (MACE) technique has been widely used to prepare ultrathin NWs with no impurities, due to its simplicity, low operating temperature, and low cost [26]. Pt, Au, Pd, Cu, and Ni depositions on silicon wafers in HF solutions have been extensively studied [27-29]. MACE is a localized microelectrochemical redox reaction process in which both anodic and cathodic processes occur simultaneously on the silicon surface, these processes involve the spontaneous oxidation of silicon atoms and the reduction of metal ions to metallic particles in the absence of an external source of electric current. The morphologies of Si NWs can be affected by many

factors, such as the doping type, doping level, orientation of the silicon wafers, concentration of H_2O_2 in the etchant, and etching temperature [30].

Recently, Voigt et al. reported that Si NWs prepared by using MACE emit PL at visible wavelengths [31]. However, the cause of the PL from the prepared Si NWs was not clearly stated. To determine the origin of the PL from the Si NWs, we fabricated luminescent Si NWs by using the MACE technique and analyzed the optical emission properties of the Si NWs by using PL measurements at various temperatures (5 K ~ 300 K).

2.2. Experiments

The preparation of the luminescent Si NWs was similar those previously reported [32], but with slight modification. The silicon wafers were cut into 10 mm^2 pieces and cleaned by rinsing them in acetone for 2 min, followed by an ethanol rinse for another 2 min. Native SiO_2 removal was carried out by briefly dipping in a 48% HF solution, followed by 2% HF rinsing for 1 min. Finally, the samples were rinsed in deionized water and blow-dried with nitrogen. This cleaning procedure yields hydrogen-terminated silicon surfaces (for a limited time of a few minutes), which allows for subsequent silver deposition on oxide-free surfaces of the silicon wafers.

Ag nanoparticles were spin-coated on to the silicon wafer by using a Ag-coating solution containing 4.8 M HF and 0.04 M $AgNO_3$. After the Ag-nanoparticle coating, the silicon wafer was washed with water to remove excess Ag^+ ions and then immersed in an oxidizing HF etching solution composed of 4.8-M HF and 30% H_2O_2 (9:1 v/v) in a reaction vessel. After the etching at room temperature, the Si NWs were washed repeatedly with water and then immersed in dilute HNO_3 (1:1 v/v) to dissolve the Ag catalyst. The Si NW samples were rinsed with deionized water and dried at room temperature; their surfaces were colored deep black, and their rear sides were colored gray. For the Si NWs to be used for luminescence measurement, the prepared Si NWs was stored at room temperature for 60 h.

Steady-state PL spectra were obtained using an Ocean Optics S2000 spectrometer (Ocean Optics, Inc., Dunedin, FL, USA) fitted with a fiber optic probe. A tungsten light source and UV light-emitting diode (LED) (λ max = 400 nm) were used to obtain reflectivity and PL spectra, respectively. The illumination of the surface and the detection of the reflected and transmitted PL light were recorded with a CCD detector in the wavelength range from 400 to 1200 nm. To obtain high-resolution transmission electron microscopy (HR-TEM) (a Philips TECNAI F20 microscope) images, sonicated the Si NWs in ethanol. The HR-TEM specimens were prepared by dipping carbon micro-grids (Ted Pella Inc., 200 Mesh Copper Grid) into the ethanol solution, and the microscope was operated at 200 keV.

For temperature-dependent PL measurements, a 50 cm spectrograph taken with a liquid-nitrogen-cooled charge-coupled device was used to measure the PL emission spectrum. The spectral resolution of the spectrometer was < 0.1 meV when using a 1200 line/mm grating. The 442 nm line of a HeCd laser was used as the ultraviolet (UV) excitation source. Low-temperature PL measurements were carried out at temperatures between 5 K and 300 K by using a closed-cycle 4He refrigerator. To analyze the PL spectra, we adopted a multiple oscillator fitting technique to separate energetically closely located emission peaks.

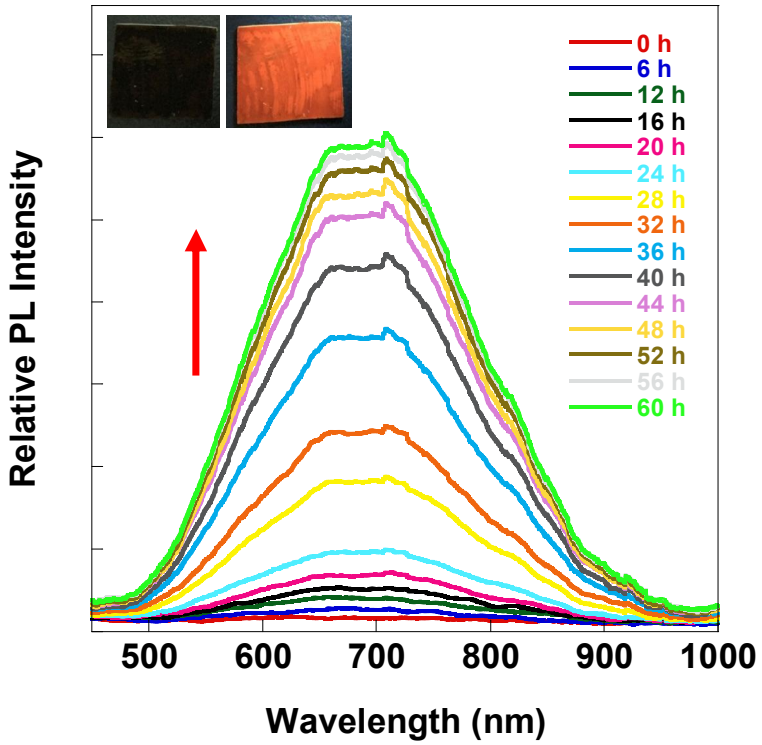

Fig. 2.1. Evolution of the PL from the Si NWs. The insets show photographs of the Si NWs under white light (left).

2.3. Results and Discussion

The PL spectra of the Si NWs were measured at room temperature, and the emission spectra were collected at an excitation wavelength of 400 nm. The luminescent Si NW samples were prepared by using MACE and placed at room temperature for 60 h. Figure 1 shows the steady-state PL spectra of Si NWs and indicates that the maximum emission intensity was centered at 700 nm for an excitation wavelength of 400 nm. The PL intensity for the Si NWS increased gradually during air exposure and reached maximum in 60 h. An emission at 700 nm did not shift with increasing exposure time. The photographs of the Si NWs under white light (left) and under UV light (right), which are shown in the inset, indicate that the PL from the Si NWs is visible to the naked eye.

The top-view and the cross-sectional morphologies of the Si NWs shown in Fig. 2 were obtained using scanning electron microscopy (SEM). The top view of the Si NWs shows that the Si NWs were aggregated in bundles. The cross-sectional image of the Si NWs illustrates that the lengths of the Si NWs were about 25 μm. The diameters of Si NWs were about a few hundreds of nanometers.

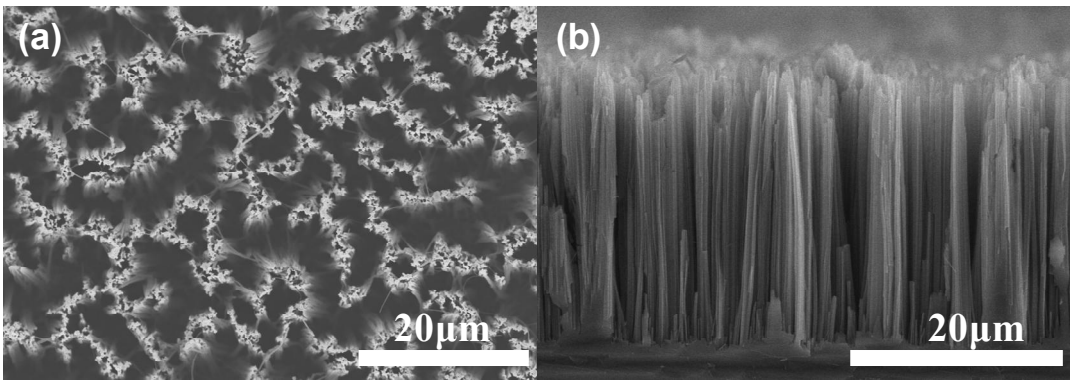

Fig. 2.2. Surface and cross-sectional SEM images of the Si NWs.

To determine the origin of the PL, we prepared two different samples of Si NWs. One is the Si

NWs sample right after MACE, which does not luminesce, and the other is the luminescent Si NWs stored at room temperature for 60 h. To obtain the morphology of a single Si NW, we ultra-sonicated the samples to detach a single Si NW from the silicon substrate. Figure 3 shows high-resolution images of two different types of Si NWs. The Si NWs right after MACE shown in Fig. 3(a) have a thin rough surface on a solid core; however, the luminescent Si NWs shown in Fig. 3(b) have a few nm-sized particles on the surface of the solid core.

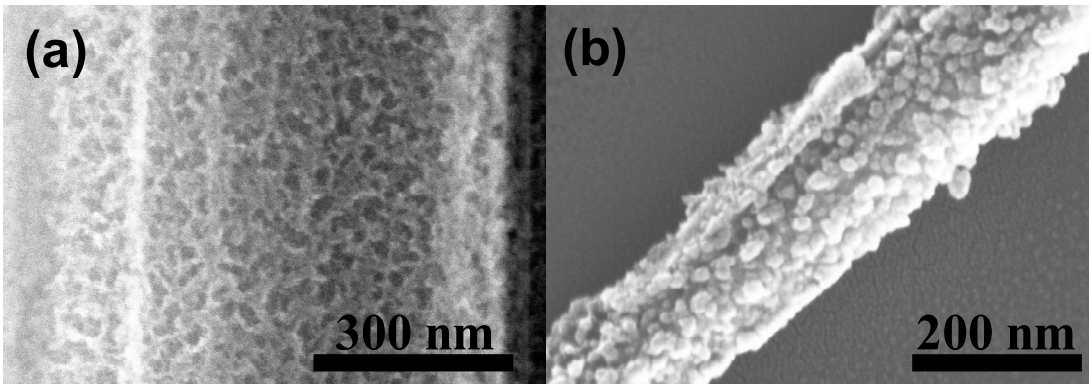

Fig. 2.3. High-resolution SEM images of (a) a non-luminescent Si NW and (b) a luminescent Si NW.

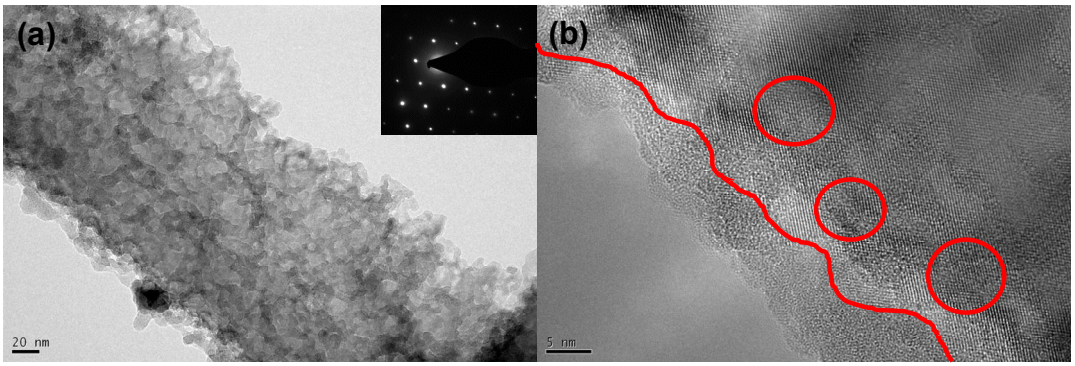

Fig. 2.4. HR-TEM images of a luminescent Si NW. The inset shows the selected area electron diffraction patterns.

Figure 4 shows HR-TEM images of a luminescent Si NW; these images indicate that the surface of the Si NW is very rough and that a few nano-sized silicon particles are attached to the Si NW, which is different from the results previously reported for porous Si NWs [32]. The selected area electron diffraction patterns (insets), confirm the single-crystalline nature of the Si NW. The lattice plane image shows a typical Si (100) structure, and the measured d spacing is 2.86 Å for the (100). An enlarged HR-TEM image of the edge surface of the Si NW reveals that the edge surface has the amorphous structure of silicon oxide due to oxidation of the Si NW by the oxygen in the ambient air. The circles in HR-TEM image indicate the silicon nanoparticles.

To investigate the origin of the PL, we obtained measurements at temperatures from 5 K to room temperature, and the results are shown in Fig. 5. The PL spectra of the Si NWs were taken in steps 20 K and are shown in Fig. 5(a). In Fig. 5(a), no pattern of PL can be seen; however Fig. 5(b) and (c) indicate that the PL intensity decreases and that the wavelength of the PL shifts to shorter wavelength as the temperature is increased. The thermal quenching behavior of the PL emission intensity for the Si NW sample is due to surface states. During the oxidation process, the luminescent Si NWs contain appreciable numbers of surface states. These surface states may form surface excitons. Normally, these surface exciton transitions quench with increasing temperature [33].

The Raman spectra of the non-luminescent Si NWs and the luminescent Si NWs are shown in Fig. 6. The Raman peak at 528.9 cm^{-1} with a full width at half maximum (FWHM) of 12.9 cm^{-1} can be seen in the Raman spectrum of the non-luminescent Si NWs and can be attributed to scattering of the first-order optical phonon (TO) of Si NWs. In comparison, the first-order Raman peak of the luminescent Si NWs is at 523.1 cm^{-1} with an FWHM of 21.6 cm^{-1} (a downshift by 5.8 cm^{-1}). Its linewidth is broadened and the line shape becomes increasingly asymmetric with an extended tail at low frequencies (Fig. 6 inset). Qualitatively, when the crystalline size decreases, momentum conservation will be relaxed ($q \neq 0$) and Raman-active modes will not be limited to being at the center of the Brillouin zone (G point). The smaller the

crystalline grain, the larger is the frequency shift and the more asymmetric and broader the peak becomes, which is due to quantum confinement phenomena [34]. This quantum confinement has been proven by experiments on nanocrystalline silicon [35] and porous silicon [36] and an Si NWs fabricated by using thermal evaporation [37].

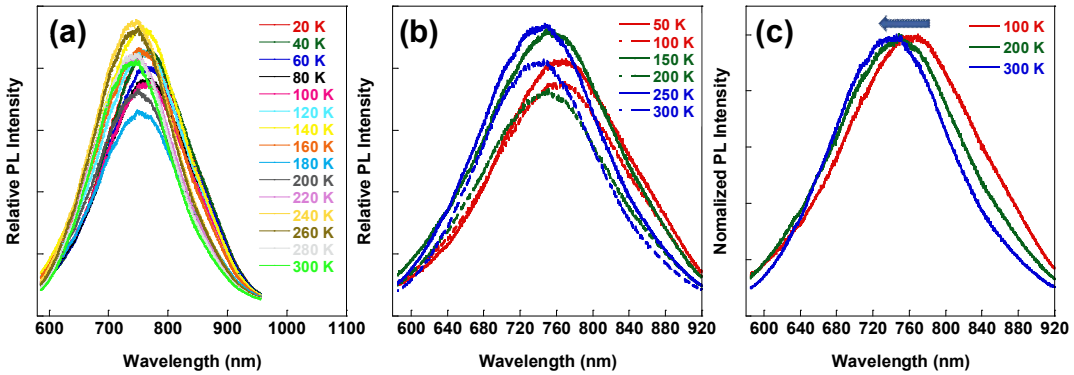

Fig. 2.5. Temperature dependence of the PL spectra from Si NWs.

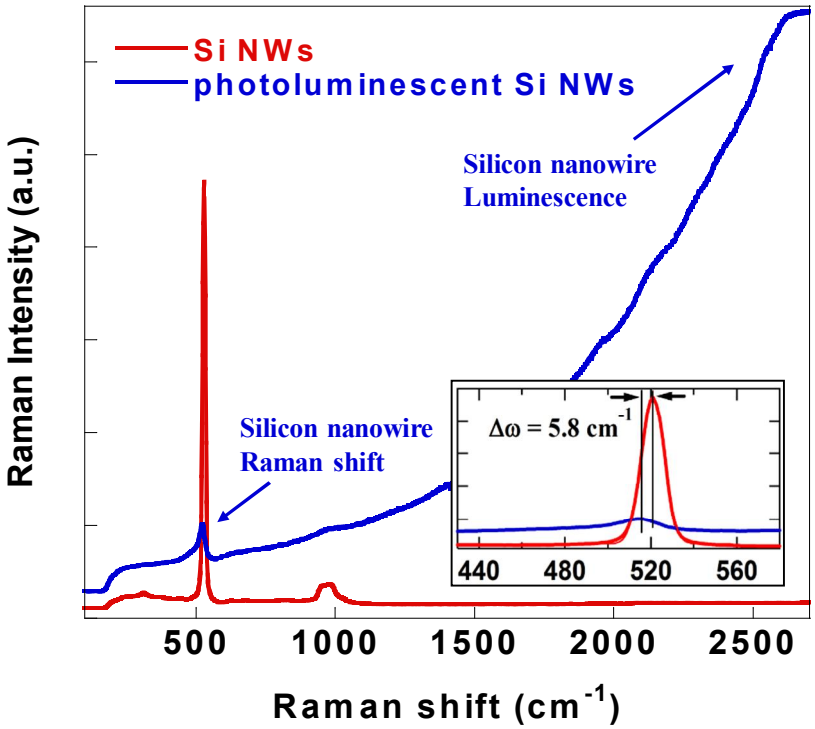

Fig. 2.6. Raman spectra of non-luminescent and luminescent Si NWs. The inset shows that the first-order Raman peak of the luminescent Si NWs is downshifted by 5.8 cm^{-1}.

2.4. Conclusion

The origin of the PL from the Si NWs was investigated, and their optical properties were characterized by using PL and Raman measurements. The PL intensity decreases in the temperature-dependent PL spectroscopy and that the wavelength of the PL shifts to shorter wavelength as the temperature is increased. This result is due to the oxidation process of the Si NWs. The Raman spectra of non-luminescent Si NWs and luminescent Si NWs were investigated and the line width were found to be broadened and the line shapes to become asymmetric with an extended tail at low frequencies for the luminescent Si NWs, which is due to quantum confinement phenomena. HR-TEM images of the luminescent Si NW show that a few nano-sized silicon particles, which may be caused luminescence property are attached to the Si NW.

2.5. References

[1] D. Ma, C. Lee, F. Au, S. Tong and S. Lee, *Science* **299**, 1874 (2003).

[2] Y. Cui and C. M. Lieber, *Science* **291**, 851 (2001).

[3] Y. Huang, X. Duan, Y. Cui, L. J. Lauhon, K.-H. Kim, and C. M. Lieber, *Science* **294**, 1313 (2001).

[4] A. Cullis and L. T. Canham, *Nature* **353**, 335 (1991).

[5] L. T. Canham, *Appl. Phys. Lett.* **57**, 1046 (1990).

[6] J. Valenta, B. Bruhn and J. Linnros, *Nano Lett*. **11**, 3003 (2011).

[7] X. Lu, C. M. Hessel, Y. Yu, T. D. Bogart and B. A. Korgel, *Nano Lett.* **13**, 3101 (2013).

[8] A. R. Guichard, D. N. Barsic, S. Sharma, T. I. Kamins and M. L. Brongersma, *Nano Lett.* **6**, 2140 (2006).

[9] J. Wilcoxon and G. Samara, *Appl. Phys. Lett.* **74**, 3164 (1999).

[10] G. Ledoux, J. Gong, F. Huisken, O. Guillois and C. Reynaud, *Appl. Phys. Lett.* **80**, 4834 (2002).

[11] A. I. Hochbaum, R. Chen, R. D. Delgado, W. Liang, E. C. Garnett, M. Najarian, A. Majumdar, and P. Yang, *Nature* **451**, 163 (2008).

[12] B. Tian, X. Zheng, T. J. Kempa, Y. Fang, N. Yu, G. Yu, J. Huang, and C. M. Lieber, *Nature* **449**, 885 (2007).

[13] E. C. Garnett and P. Yang, *J. Am. Chem. Soc.* **130**, 9224 (2008).

[14] M. D. Kelzenberg, D. B. Turner-Evans, B. M. Kayes, M. A. Filler, M. C. Putnam, N. S. Lewis, and H. A. Atwater, *Nano Lett.* **8**, 710 (2008).

[15] K. Bhowmik and A. Mondal, *Electron. Mater. Lett.* **11**, 180 (2015).

[16] C. K. Chan, H. Peng, G. Liu, K. McIlwrath, X. F. Zhang, R. A. Huggins, and Y. Cui, *Nat. Nanotechnol.* **3**, 31 (2008).

[17] G. Zheng, F. Patolsky, Y. Cui, W. U. Wang, and C. M. Lieber, *Nat. Biotechnol.* **23**, 1294 (2005).

[18] S. M. Koo, Q. Li, M. D. Edelstein, C. A. Richter, and E. M. Vogel, *Nano Lett.* **5**, 2519

(2005).

[19] Y. Cui, Z. Zhong, D. Wang, W. U. Wang, and C. M. Lieber, *Nano Lett.* **3**, 149 (2003).

[20] X. F. Duan, Y. Huang, and C. M. Lieber, *Nano Lett.* **2**, 487 (2002).

[21] R. S. Wagner and W. C. Ellis, *Appl. Phys. Lett.* **4**, 89 (1964).

[22] H. F. Yan, Y. J. Xing, Q. L. Hang, D. P. Yu, Y. P. Wang, J. Xu, Z. H. Xi and S. Q. Feng, *Chem. Phys. Lett.* **323**, 224 (2000).

[23] D. P. Yu, Y. J. Xing, Q. L. Hang, H. F. Yan, J. Xu, Z. H. Xi and S. Q. Feng, *Physica E* **9**, 305 (2001).

[24] Y. Wang, V. Schmidt, S. Senz and U. Gosele, *Nat. Nanotechnol.* **1**, 186 (2006).

[25] B. Fuhrmann, H. S. Leipner, H.-R. Höche, L. Schubert, P. Werner and U. Gösele, *Nano Lett.* **5**, 2524 (2005).

[26] T. Kawashima, T. Mizutani, T. Nakagawa, H. Torii, T. Saitoh, K. Komori and M. Fujii, *Nano Lett.* **8**, 362 (2008).

[27] K. Q. Peng, Y. J. Yan, S. P. Gao and J. Zhu, *Adv. Mater.* **14**, 1164 (2002).

[28] K. Peng, J. Hu, Y. Yan, Y. Wu, H. Fang, Y. Xu, S. Lee and J. Zhu, *Adv. Funct. Mater.* **16**, 387 (2006).

[29] K. Peng, Y. Xu, Y. Wu, Y. Yan, S. T. Lee and J. Zhu, *Small* **1**, 1062 (2005).

[30] Z. Huang, N. Geyer, P. Werner, J. D. Boor and U. Gösele, *Adv. Mater.* **23**, 285 (2011).

[31] F. Voigt, V. Sivakov, V. Gerliz, G. H. Bauer, B. Hoffmann, G. Z. Radnoczi, B. Pecz and S. Christiansen, *Phys. Status Solidi A* **208**, 893 (2011).

[32] D. Jung, S. G. Cho, T. Moon and H. Sohn, *Electron. Mater. Lett.* **12**, 17 (2016).

[33] J. Grawboska, M. Meaney, K. K. Nanda, J.-P. Mosnier, M. O. Henry, J.-R. Duclere and E. McGlynn, *Phys. Rev. B* **71**, 115439 (2005).

[34] K. W. Adu, Q. Xiong, H. R. Gutierrez, G. Chen and P. C. Eklund, *Appl. Phys. A-Mater. Sci. Process.* **85**, 287 (2006).

[35] Z. Iqbal and S. Veperk, *J. Phys. C* **15**, 377 (1982).

[36] Z. F. Sui, P. P. Leong, I. P. Herman, G. S. Higashi and H. Temkin, *Appl. Phys. Lett.* **60**, 2086 (1992).

[37] D. P. Yu, Z. G. Bai, Y. Ding, Q. L. Hang, H. Z. Zhang, J. J. Wang, Y. H. Zou, W. Qian, G. C. Xiong, H. T. Zhou and S. Q. Feng, *Appl. Phys. Lett.* **72**, 3458 (1998).